High-Power Sodium Titanate Anodes; A Comparison of Lithium vs Sodium-ion Batteries

Yijie Xu[†,††], Dustin Bauer[†], Mechthild Lübke[†], Thomas Ashton[†], Yun Zong[††], and Jawwad A. Darr[†*]

[†]Department of Chemistry, University College London, 20 Gordon Street, London WC1H 0AJ, United Kingdom

[††] Institute of Materials Research and Engineering, A*STAR (Agency for Science, Technology and Research), 2 Fusionopolis Way, 138634, Singapore

*Corresponding Author

Email: j.a.darr@ucl.ac.uk

Abstract: Sodium titanate nanopowder (nominal formula $Na_{1.5}H_{0.5}Ti_3O_7$) is directly synthesized using a continuous hydrothermal flow synthesis process using a relatively low base concentration (4 M NaOH) in process. The as-made titanate nanomaterials are characterised using powder X-ray diffraction, X-ray photoelectron spectroscopy, energy-dispersive X-ray spectroscopy, Raman spectroscopy, Brunauer–Emmett–Teller analysis, and transmission electron microscopy, evaluated as potential electrode materials for Li-ion and Na-ion batteries. Cyclic voltammetry studies on half-cells reveal that the sodium titanate nanomaterial stores charge primarily through a combination of pseudocapacitive and diffusion-limited mechanisms in both systems. Electrochemical cycling tests at a high specific current of 1000 mA g^{-1}, reveal that the Li-ion and Na-ion cells retained relatively high specific capacities of 131 and 87 $mAhg^{-1}$, respectively, after 400 cycles. This study demonstrates the potential of CHFS-made sodium titanate nanopower as anode material for Li and Na ion cell chemistries.

Keywords: Continuous hydrothermal flow synthesis; Sodium titanate; $Na_2Ti_3O_7$; Na-ion battery; Li-ion battery, High power

Graphical Abstract

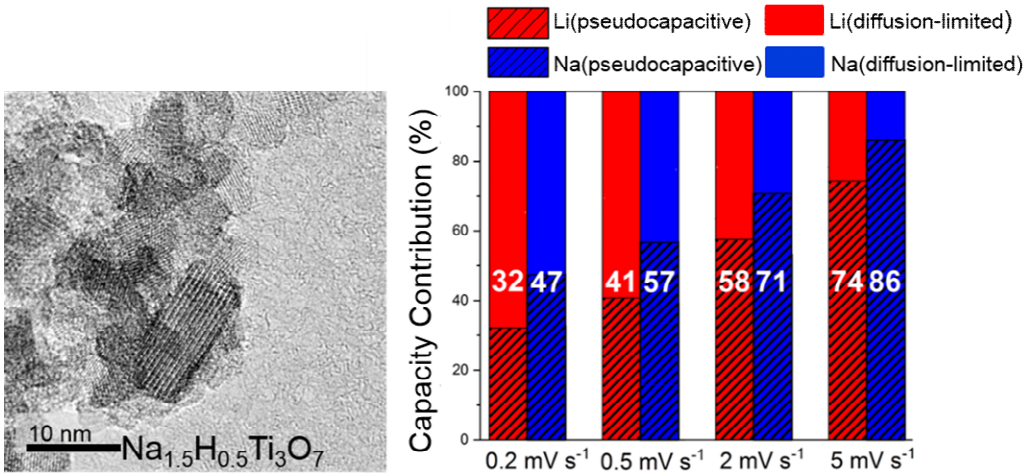

1. Introduction

The increasing demand for energy, along with public concerns over the effects of emissions from burning of fossil fuels, have led to interest in developing renewable and efficient energy technologies.[1] In particular, developing more sustainable smart grid energy storage devices for solar and wind energy harvesting sources, has become important in coping with peak energy supply and demand issues.[2] Since the commercialization of rechargeable Li-ion batteries by Sony in 1991, the technology has become the dominant energy storage approach in many portable devices due to their high energy densities.[3] With the increasing costs of lithium, attention has shifted to finding more readily-accessible, inexpensive, and environmentally friendly alternative charge carriers such as Na-ions.[4] The apparent similarities of some of the insertion chemistry for Li- and Na-ions, allows for expertise from existing Li-ion battery research to be transferred and hence, progress in Na-ion batteries could be accelerated.[5, 6] Furthermore, elemental sodium can readily be easily extracted from natural sources such as seawater or from molten sodium hydroxide through electrolysis via the Downs[7] and the Castner[8] processes, respectively.[9]

The energy storage mechanisms of electrode materials for both Na- and Li-ion systems can be generalized into either insertion, alloying, or conversion-based processes. Intercalation/insertion-based materials possess the ability to accommodate ions within their structures via n-dimensional channels (where n is in the range 1 to 3).[10] However, due to its larger ionic radius, Na-ions require a spacing of 3.7 Å for smooth intercalation/extraction which is not satisfied by traditional Li-ion anode hosts, *e.g.* graphite.[11] For example, the interlayer distance between graphene sheets is typically 3.35 Å, whilst the diameter of a Na-ions is ca. 2.0 Å (compared to 1.5 Å for Li-ions), resulting in possible effects on long-term cycling stability.[12, 13] Hence, efforts have been made to find suitable Na-ion anode materials, with candidates including hard carbons,[14] transition metal oxides[15] (including spinels[16]), phosphates, phosphides and sulphides.[17] Of these, metal titanate materials tend to show promise for Na-ion batteries due to the low cost and high natural abundance of titania, good thermal stability and a preference for forming layered structures with suitably wide crystal lattice spacing which favours insertion processes.[6]

Sodium titanates of the form $Na_2Ti_nO_{2n+1}$, are characterized by zig-zagged edge- and corner- sharing TiO_6 octahedra that form sheet layers with intercalating Na-ions located between them.[18] Sodium titanates based on the generic formula $Na_2Ti_3O_7$, can possess a large interlayer spacing (of as large as ca. 8 Å), which can potentially facilitate excellent cycling performance in both Li- and Na-ion batteries, particularly under high-power conditions,[18] while possessing higher power densities than graphite.[19] These materials also possess one of the lowest insertion voltages for Na-ion cells at ca. 0.3 V *vs.* Na/Na^+ (versus ca. 1.7 V for Li^+/Li for Li-ion cells [20]) and a high theoretical capacity of 177 mAh g^{-1} for Na-ion.[21] Furthermore, the inherent layered structure of such titanates is ideal in tolerating large volume changes that occur during cycling, resulting in more stable cycling performance.[22] Thus, $Na_2Ti_3O_7$ -based structures possess favourable characteristics that make them potentially suitable anode materials for large-scale grid-storage applications.[23] Nano-sizing of battery electrode materials can increase rate performance by improving ion access to intercalation channels by virtue of a higher surface area to volume ratio.[23] In addition, it has been shown that with higher surface area, a higher surface capacitive contribution can be observed, often resulting in greater specific stored charge capacity at high specific current.[24]

Previous attempts in the literature to synthesize sodium titanates via batch hydrothermal approaches, have produced a diverse range of phases and particle morphologies, with titanate products of the nominal formulae $Na_2Ti_3O_7$, and $NaTi_3O_6(OH)\cdot 2H_2O$, being made at base concentrations of 10 and 11 M, respectively.[19, 25] However, conventional batch hydrothermal methods, may have some disadvantages such as batch to batch variations, long reaction times, energy or chemically intensive syntheses and often poor control over particle properties such as size, shape, and morphology.[26]

In contrast to conventional batch hydrothermal or solvothermal synthesis methods, continuous hydrothermal flow synthesis (CHFS) methods allow for rapid production of inorganic nanomaterials, offering fast reaction kinetics and some control over particle properties.[27] The continuous hydrothermal synthesis process as developed by the authors is based on introducing one or more metal salt solution feeds with a flow of supercritical water (typically the latter is at a temperature of ca. 450°C and a pressure of 24.1 MPa) inside a specially engineered mixer. The resulting sudden changes in

conditions experienced by the metal salts, results in the instant formation of nanocrystals via complex simultaneous reactions (largely hydrolysis, degradation and dehydration reactions).[28] Successful examples of CHFS-made products include different metal oxides[15, 29, 30] (including spinels[16]), phosphates,[31] and nitrides.[32] The inherent capability to alter and control parameters in CHFS (such as flow rates, concentrations, pH, temperature and pressure) allows for product consistency and some tunability over the final particle attributes to be obtained.[27] Consequently, CHFS-type processes have attracted industry attention as demonstrated by the first commercial reactor that was commissioned by Hanwha Chemicals of Korea in 2010.[33]

Previous reports[23, 34] detailing the synthesis of sodium titanate via CHFS by the authors, used relatively high concentrations of NaOH base (in the range 12 to 15 M) with the titanium containing precursor typically in the range 0.2 to 0.3 M, resulting in nano-sized sheet-like morphologies being observed without the presence of individual small or fine nanoparticles or clusters. In more recent studies, the sodium titanate synthesized at 12 M NaOH via CHFS was determined to be $H_{1.1}Na_{0.9}Ti_3O_7$.[23] This material was shown to possess excellent electrochemical performance in Li-ion half-cells vs. Li metal at moderate specific currents, displaying a specific capacity of 120 mAh g^{-1} at a specific current of 500 mA g^{-1}. During that time, the authors were not aware of comparable literature on a synthesis (or electrochemical properties) of similar sodium titanates made in flow using base concentrations below 5 M. Under lower base concentrations, it would be expected that either anatase or smaller 2D nano-sheets of sodium titanate phases might be formed in flow; if the latter could be achieved, it would be useful to explore their electrochemical properties in both Li- and Na-ion batteries.

Herein, the authors describe the direct and continuous hydrothermal flow synthesis (CHFS) of a layered sodium titanate nanomaterial, synthesized at a previously unreported sustainable base concentration (4 M NaOH), which was then investigated as an electrode material in both Na and Li-ion batteries.

2. Experimental

2.1 Synthesis

Sodium titanate nanopowders were synthesised using a continuous hydrothermal flow synthesis (CHFS) reactor incorporating a confined jet mixer, CJM (patent no US 9192901, Figure S1 in the Supplementary Information), that was designed to facilitate highly efficient mixing and eliminate blockages under these conditions.[16, 35-46] A co-current CJM was made from off-the-shelf Swagelok™ parts and allowed for efficient mixing of a supercritical water stream with a (pre-mixed) ambient temperature aqueous metal salt solution stream.[47] Herein, the authors used a laboratory scale CHFS reactor, which is similar design to the pilot scale CHFS process described in previous publications,[38, 39] but at ca. one fifth of the pilot plant scale.[48]

The general hydrothermal flow reactor set-up was as follows: three identical pumps (Primeroyal K, Milton Roy, France) were used to supply three independent feeds, which were pressurised to 24.1 MPa. An aqueous solution of 0.1 M TiBALD (precursor 1) was supplied at a flow rate of 40 mL min^{-1} by pump 1. A second aqueous feed of 4 M NaOH base and 1 M $NaNO_3$ (precursor 2) was supplied at a flow rate of 40 mL min^{-1} by pump 2, leading to a ca. 40× excess of Na-ions to titanium ions in order to maximize sodium uptake. Within the CHFS process, these two precursor feeds were premixed in flow at room temperature (inside a dead volume tee piece) and then this combined mixture was then mixed with a flow of supercritical water inside a patented confined jet mixer (patent no US 9192901), which is designed to facilitate highly efficient mixing while minimizing blockage.[16, 35, 40-46, 49] The latter feed of supercritical water was produced by pumping ambient temperature feed of water at 80 mL min^{-1} and heating it in flow to reach a temperature of ca. 450 °C (at 24.1 MPa).

The reaction residence time (after mixing) was calculated to be ca. 3 s at a reaction temperature of 335 °C. The newly formed particles were then cooled in process using a pipe-in-pipe heat exchanger, before they passed through a back-pressure regulator and were collected at ca. 40 °C. Thereafter, the white nanopowder laden slurry was cleaned by allowing the solids to sediment under gravity for 2 hours before washing briefly in pH 8 ammonia solution to prevent Na-ions leeching and maximize electrochemical performance.[50] The resulting wet solids were then freeze-dried (Virtis Genesis 35XL) by warming the samples from -60 to 25 °C for 24 h under a vacuum of <13.3 Pa, resulting in free-flowing powders. The as-synthesized freeze-dried powders were heat treated at 150, 300, 450, or 800 °C, respectively (Fig. S3).

2.2 Materials Characterisation

Powder X-ray diffraction (XRD) patterns of the samples were collected over the 2θ range of 2 to 45° with a step size of 0.5 ° and step time of 10 s on a STOE diffractometer using Mo-Kα radiation (λ = 0.7093 Å). Crystallite sizes were estimated from the XRD data using the Scherrer equation[51], $K\lambda/\beta\cos\theta$, where K is the shape dimension factor, λ the wavelength of the incident radiation source, β the width of the diffraction peak at half maximum intensity (following correction for instrumental broadening), and θ the Bragg angle value of diffraction (in degrees). Surface elemental composition was determined using X-ray photoelectron spectroscopy (XPS) collected on a Thermo Scientific K-alpha™ spectrometer using Al-Kα radiation. High-resolution regional scans for the Ti 2p, O 1s, C 1s, and Na 1s were conducted at 50 eV. Processing of the XPS data was performed using CasaXPS™ software (version 2.3.16) and by calibrating the spectra using the adventitious C 1s peak at 284.7 eV.

High-resolution transmission electron microscopy (TEM) using a Jeol JEM 2100 TEM fitted with a LaB_6 filament was used to determine the crystallite size, interlayer spacing, and morphologies. A Gatan Orius digital camera for digital image capture of the sodium titanate sample which was prepared by ultrasonically dispersing the powder in > 99.5 % pure methanol (EMPLURA, Darmstadt, Germany) and pipetting on to a copper film grid (300 mesh Agar Scientific, Stansted, UK). The same TEM set-up was used to investigate the elemental composition of the sodium titanate nanopowders via energy-dispersive X-ray spectroscopy (EDS).

Brunauer-Emmet-Teller (BET) surface area measurements of the powders were carried out using liquid N_2 in a Micrometrics ASAP 2420 instrument. The sample was degassed at 150 °C (12 h) under flowing nitrogen before measurement. Raman spectra of the powders were collected with a Renishaw inVia™ Raman microscope utilizing a laser excitation source with a wavelength of 514 nm. The sample was prepared into an ethanol dispersion before being drop-cast on to silicon plate, and then allowed to dry in air for 2 h before measurement. Thermogravimetric analysis (TGA) was performed using a Pyris1 TGA instrument (Perkin Elmer) under air with a flow rate of 20 mL min^{-1} in the temperature range of 25 to 1000 °C with a heating rate of 10 °C min^{-1}.

2.3 Electrochemical characterisation

The electrodes were prepared by mixing the as-synthesized (or heat-treated) titanate nanopowder active material with conducting carbon black (Super P, Alfa Aesar, Heysham, UK) and binder agents (polyvinylidene fluoride binder, PVDF, PI-KEM, Staffordshire, UK) at a wt% ratio of 70:20:10. A 10 wt% solution of PVDF was prepared by dissolving the solid in NMP (N-methyl-2-pyrrolidone, Sigma Aldrich, St. Louis, USA) for at least 1 h at room temperature, before adding the active material and conductive agent. The mixtures were milled briefly in a planetary mill (Pulverisette 7, Fritsch) at 800 rpm for 20 minutes, before the doctor-blading on to aluminium and copper foil (PI-KEM, Staffordshire, UK) at a thickness of ca. 110 microns for Na-ion and Li-ion cells, respectively. Electrodes with a diameter of 16 mm were punched out, pressed under 1.5 tons of pressure and finally dried overnight at 70 °C in a vacuum oven. The electrodes had an active material mass loading in the range of 1.0 to 1.1 mg cm^{-2}. Electrochemical half-cell tests were performed using two-electrode 2032-type coin cells, which were assembled in an argon-filled glovebox with O_2 and H_2O level below 0.50 ppm. The counter electrode was either sodium metal foil (PI-KEM, Staffordshire, UK) or a lithium metal chip (PI-KEM, Staffordshire, UK), with a glass microfiber filter (Whatman, Buckinghamshire, UK) serving as a separator. The cell was infused with 1 M $NaPF_6$ or $LiPF_6$ in 3:7 wt% ethylene carbonate/ethyl diethylcarbonate (Kishida Chemicals, Osaka, Japan) as electrolyte.

Constant current charge-discharge, cyclic voltammetry and specific current rate testing of Na-ion and Li-ion half-cells were performed using a 48-channel Arbin Instrument (Caltest Instruments Ltd, Guildford, UK) at room temperature. Cyclic voltammetry (CV) measurements were performed in the potential range 0.1 to 2.5 V (vs. Na/Na^+ and Li/Li^+) at scan rates of 0.05, 0.2 0.5, 2, and 5 mV s^{-1}, respectively. Galvanostatic charge-discharge cycling was performed in the potential range 0.1 to 2.0 V vs. Na/Na^+ and 0.1 to 2.5 V vs. Li/Li^+ at a specific current of 100 mA g^{-1} during charge and discharge, respectively. The specific current test was performed at specific currents of 50, 100, 200, 500, 750, 1000, and 2000 mA g^{-1}.

3. Results and Discussion

3.1 Physical Characterisation Results

The as-synthesized (and freeze-dried) sample was obtained as an off-white powder at a production rate of 62 g per hour, with a yield of >86 % (based on the titanium precursor concentration), which can be explained by losses from post-synthesis washing (this rate could be scaled-up in the future to >300 g per hour by utilizing a scaled up CHFS pilot plant operated by the UCL authours).[27] Powder XRD patterns for sodium titanates such as $Na_2Ti_3O_7$ have been previously reported.[19, 52] The powder XRD pattern of the as-synthesized sample (see Figure 1a), showed good agreement to the XRD reference pattern ($Na_2Ti_3O_7$; JCPDS 31-1329), with characteristic peaks being observed at 2θ = 4.0° (001), 11.2° (011), 13.1° (111), 20.0° (401), 21.6° (020) and 29.5° (421). The relatively intense peak at 2θ = 4.0°, suggested some preferential growth in the particles, which has been observed previously for similar materials in sheet-like form; the position of this peak is also known to shift depending on interlayer spacing, which can be affected by water content for example.[53, 54] The difference in intensities observed between the experimental and reference patterns was further suggestive of preferential growth in different crystallographic directions, which could be attributed to different morphologies within the sample. Measured BET surface area was 74 m^2 g^{-1}. Thermogravimetric analysis of the as-synthesized powder (see Figure S2 in the Supplementary Information) revealed a ca. 5 % weight loss in the temperature range of 25 to 150 °C, which was attributed the loss of weakly adsorbed and strongly bonded water. A small mass loss in the temperature range of 200 to 400 °C was attributed to the dehydroxylation of intralayer -OH groups.[55] A further weight loss of 2.5 % was observed in the range of 600 to 800 °C and attributed to the decomposition and structural rearrangement into the $Na_2Ti_7O_{15}$ phase (see Figure S3 in the Supplementary Information).[19] This is supported by the corresponding DSC pattern, which displayed a large endothermic process in the temperature range of 450 to 780 °C ; this has previously been attributed to the formation of new Ti-O-Ti bonds.[56] Literature reports have suggested that heat-treatment of such sodium titanates can result in a decrease in the Na:Ti ratio of the resulting

titanate phase (e.g. change in the ratio from 1:1.5 to 1:3.5) and formation of a secondary Na_2O phase.[57, 58] These changes that typically occur in the temperature range of 500 to 600 °C have been attributed to Ti (IV) ions repositioning themselves due to a vacancies left by the initial removal of chemically bonded water and interlayer OH groups (arising from the original deficiency in Na-ions in the as-synthesized material).[19, 23, 59]

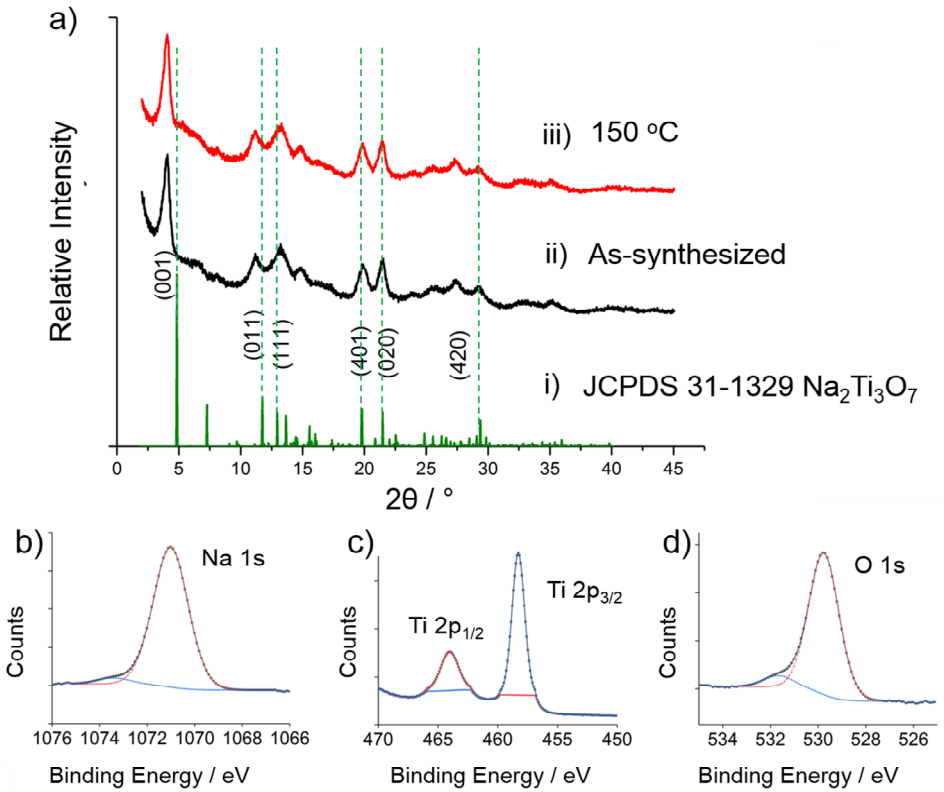

Figure 1. (a) (i) XRD line pattern for the JCPDS standard reference pattern JCPDS 31-1329 for $Na_2Ti_3O_7$, XRD patterns of (ii) as-synthesized sodium titanate synthesized at 4 M NaOH and (iii) titanate material heat treated at 150 °C. XPS spectra of as-synthesized titanate material, with spectra in the regions for (b) Na 1s (red), (c) Ti 2p ($2p_{1/2}$ in red, $2p_{3/2}$ in blue), and (d) O 1s (red), with background noise subtracted via the Shirley model.

The average crystallite size for as-synthesized titanate nanopowder made at 4 M NaOH was estimated via application of the Scherrer equation to the pronounced (001) XRD peak and was determined to be

5.3 nm, while the values derived from the less-pronounced (011) and (401) peaks were 5.2 and 5.6 nm, respectively . [60]

The valence states of the metal ions in the as-synthesized sample were determined by high-resolution X-ray photoelectron spectroscopy (Fig. 1 b-d). The position of the oxygen O 1s peak at 529.7 eV was in agreement with that Ti-O bonds, with the small shoulder at 531.6 eV (Fig. 1d, shown in blue) being attributable to surface hydroxyl Ti-OH bonds. The peak of the Na 1s orbital at 1071.0 eV was also in agreement for sodium within bulk $Na_2Ti_3O_7$.[61, 62] The Ti 2p level binding energies were ca. 458.3 and 464.0 eV for Ti $2p_{3/2}$ and Ti $2p_{1/2}$, respectively. These binding energies with a spin orbital splitting of ca. 5.7 eV, were in good agreement with the core level of Ti^{4+}, matching the oxidation state in the predicted structure of $Na_2Ti_3O_7$. In order to better understand the elemental composition, energy-dispersive X-ray spectroscopy (EDS) measurements were performed on the as-synthesized titanate sample made at 4 M NaOH (Figure S7). The analysis suggested a Na:Ti ratio of 1:2 in the bulk structure of the as-synthesized sodium titanate. This suggests that a Na-deficient titanate structure was present for the as-synthesized sample, with the balance of charge most likely being made via protons. Thus, a composition of $Na_{1.5}H_{0.5}Ti_3O_7$ was proposed as the final structure of the as-synthesized sodium titanate nanopowder.

Raman spectroscopy was used as a supplementary analysis technique to the powder XRD results in order to gain valuable structural information. The spectra for the as-synthesized nanopowder sample (see Figure S4 in the Supplementary Information) exhibited broad bands at 200, 277, 441, 647, 840, and 900 cm^{-1} that were broadly similar to literature reports for $Na_2Ti_3O_7$.[19, 58, 63] Similar spectra were observed by Zarate et al. for sodium titanates (made via batch hydrothermal reactions at 5 M NaOH), which was attributed to a metastable structure that did not possess a 2:3:7 ratio for Na:Ti:O, but may have been a protonated Na deficient form as observed herein.[63] Herein, specific, bands below 450 cm^{-1} and bands in the range of 600 to 800 cm^{-1}, can be attributed to Na-O bond vibrations and Ti-

O stretching vibrations in the distorted TiO_6 octahedra, respectively. A band at ca. 277 cm^{-1} for the as-synthesized sample corresponds to long Ti-O bonds such as those typically seen in $Na_2Ti_3O_7$. In contrast, bands in the range of 800 to 900 cm^{-1}, correspond to Ti-O bonds of low coordination; the band at ca. 900 cm^{-1} being due to singly-coordinated Ti-O bond stretching vibrations , representative of short Ti-O bond lengths (that are typically ca. 1.7 Å long).[19]

Transmission electron microscopy images of the as-synthesized titanate nanopowder suggested the presence of small nanoparticles in clusters mixed with a smaller amount of extended thin nano-sheets (Fig. 2a). The average primary crystallite size within these clusters was ca. 5 ± 0.5 nm (based on 200 particles counted, see Figure S6 in the Supplementary Information) for both titanate samples. Sheet sizes were ca. 200 nm in width (average ca. 207 ± 21 nm), and 300 nm in length (average ca. 322 ± 30 nm), with visible curling observed at sheet edges (Figure S5). In contrast, previous syntheses made at higher base concentrations (using NaOH concentrations in the range 12 to 15 M) were exclusively sheet-only morphologies.[23, 34] These observations suggested that the formation of small particles precluded growth or aggregation into larger sheets and the rate of this process was reliant on the base concentration. In this study, the use of a lower base concentration (4 M) resulted in a smaller number of nanosheets during the short synthesis time for the CHFS process.

As expected, TEM images of the sodium titanate nanopowder heat-treated at 150 °C (Fig. 2b-c) displayed similar particle morphology to the as-synthesized material. The co-existence of both nanoparticle clusters and sheets led to the observation of two separate interlayer spacings at 0.33 ± 0.05 nm (011) and 0.76 ± 0.05 nm (001), respectively. The latter spacing was relatively large for a layered metal oxide, and can be explained by the presence of substantial inter-sheet water or hydroxyl ions being present.[19, 64] However, this value was still lower than the Bragg-equation calculated spacing from the powder XRD pattern, where a 2θ value of 4.0° for the (001) peak, suggested an interlayer spacing of ca. 10 Å. This discrepancy has been previously reported as a systematic difference between TEM-observed and XRD-calculated values.[65] This difference may be due to sample dehydration from the high vacuum and electron beam perforation by the TEM instrument. The presence of particles with different morphologies and hence, different preferred orientations, may also explain the discrepancy in

peak intensities versus the reference patterns, as the experimental XRD pattern is an average taken over multiple crystallites.

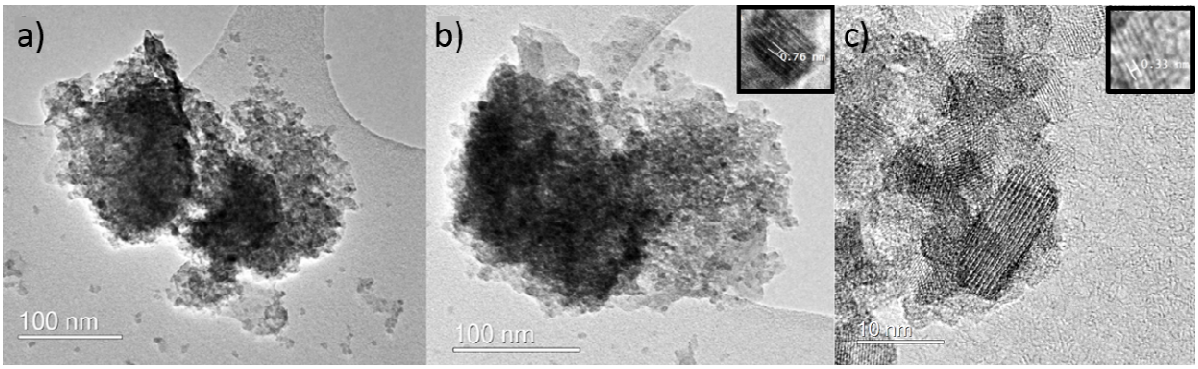

Figure 2. TEM image of (a) the as-synthesized sodium titanate nanopowder (bar = 100 nm), (b) sodium titanate heat-treated at 150 °C (inset; interlayer spacing of the same titanate nanopowder). (c) higher magnification TEM image of the sodium titanate sample heat-treated at 150 °C (bar = 10 nm) (inset; interlayer spacing of the same titanate nanopowder).

3.2 Electrochemical Characterisation Results

The charge storage properties of the $Na_{1.5}H_{0.5}Ti_3O_7$ electrodes were evaluated in Li-ion and Na-ion half-cells. In order to remove any residual or free water, the sodium titanate electrode materials were first heat-treated at 150 °C prior to use; cyclovoltammetry measurements were made on these heat-treated materials using both Li- and Na-ion half-cells; the results are displayed in Figure 3 in the potential range of 0.1 to 2.5 V vs. Li/Li^+ and Na/Na^+, respectively.

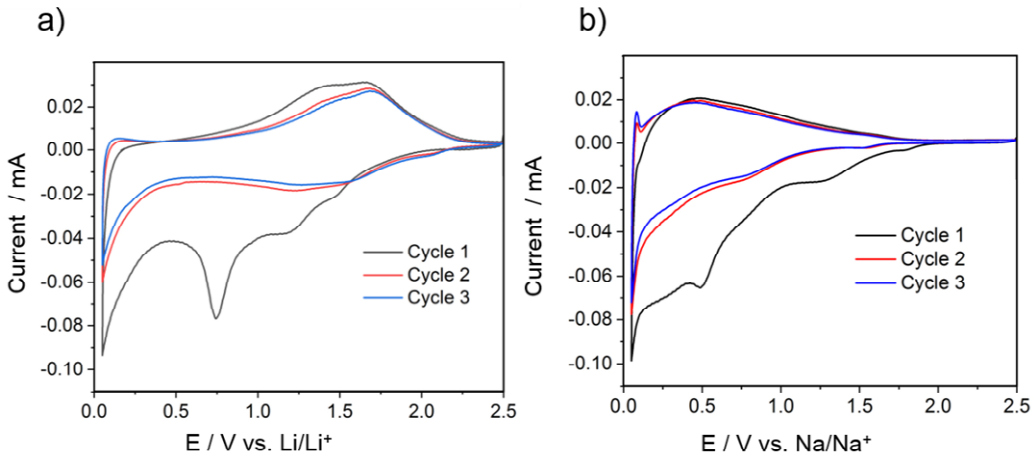

Figure 3. CVs for the first three cycles of the half cells incorporating sodium titanate (nanopowder heat-treated at 150 °C) anode, tested a scan rate of 0.05 mV s^{-1} for a (a) Li-ion half-cell and (b) Na-ion half-cell.

For the electrochemical results of the nanopowder heat-treated at 150 °C, both Li-ion and Na-ion systems showed broad and rectangular profiles with electrochemical activity taking place across wide operational potential ranges, indicative of more capacitor-like charge storage behaviour. For Li-ion half-cells, electrochemical activity occurred primarily across the potential range of 2.1 to 1 V vs. Li/Li^+, with first-cycle SEI formation coupled with irreversible carbon lithiation at 0.7 V vs. Li/Li^+. In contrast, in the Na-ion half-cell containing sodium titanate heat-treated at 150 °C exhibited electrochemical activity in the range 0.25 to 1.5 V vs. Na/Na^+, with irreversible carbon sodiation observed at ca. 0.5 V vs Na/Na^+.[19, 21] The smoothness of the cathodic insertion peak suggests a larger contribution from capacitive charge storage over insertion processes. A sharp reduction in peak area after the first cycle was attributed to the irreversible sodiation of the carbon black additive and formation of a SEI layer. The SEI layer is a permanent layer of decomposed electrolyte and electrode products that forms at the inactive and active particle surfaces during the first cycle, serving to simultaneously protect from further decomposition while hindering electron conduction due to its electronic insulating nature. [19, 66]

Scan rate tests were performed for sodium titanate heat-treated at 150 °C on both Li-ion and Na-ion cells across the same respective potential ranges as above (Figure 4) at scan rates of 0.2, 0.5, 2 and 5 mV s^{-1}. These values were chosen to allow sufficient time for ionic diffusion processes. At higher scan rates, diffusion layers are known to grow much closer to the electrode, resulting in decreased layer size and a higher flux to the electrode surface and consequently, higher current responses as observed herein.[67]

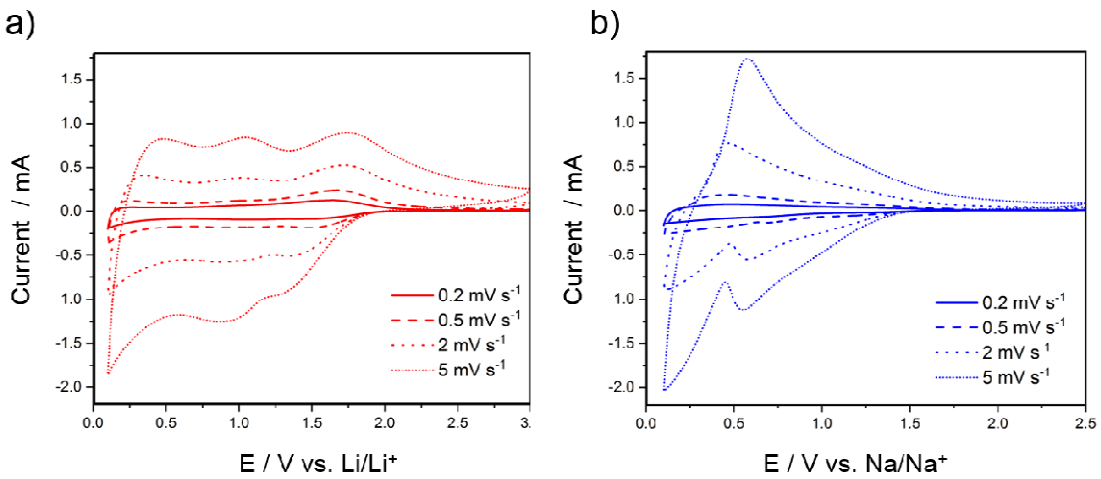

Figure 4. Cyclic voltammetry scan rate tests (at 0.2, 0.5, 2 and 5 mV s^{-1}) for half cells incorporating sodium titanate (nanopowder heat-treated at 150 °C) anodes in (a) a Li-ion half-cell vs. Li/Li^+ and (b) a Na-ion half-cell vs. Na/Na^+.

In order to better examine the percentage contribution of the pseudocapacitive and diffusion-limited charge storage mechanisms to the total volumetric charge, Trasatti's approximation method of charge storage deconvolution was utilized for the scan rates used above.[68, 69] First, the total specific charge, calculated by taking the integral of the total area under the discharge portion of the CV curve (or half of the curve area), was measured for each scan rate. The relationship between the pseudocapacitive and diffusion-limited contributions to total specific charge can be estimated as $q_t = q_c + bv^{-0.5}$, where q_t is the total specific charge of the system, q_c the pseudocapacitive contribution, and b an arbitrary constant (Equation S9). By plotting the measured peak specific capacities against the diffusion-limited

component $v^{-0.5}$, it is possible to obtain the theoretical charge contribution at infinite scan-rate (Figure 5 (a)); otherwise termed as the maximum pseudocapacitive contribution, as the y-axis intercept of the plot. From this, an estimate of the pseudocapacitive contribution can hence be expressed as $q_c/q_t \times 100\%$. The resulting ratios of charge contributions at scan rates of 0.2, 0.5, 2 and 5 mV s^{-1} for both Li- and Na-ion systems are shown in Figure 5 (b).

It can be summarized that the anode made from the sodium titanate nanopowder (heat-treated at 150 °C), displays increasing pseudocapacitive contributions with higher scan rates in both alkali-ion systems, which can be justified by the reduced time units allocated to insertion processes with larger potential steps. The relative differences between charge storage ratios across increasing scan rates suggest that both systems exhibit an increasing reliance on pseudocapacitive charge storage, with the Na-ion system exhibiting pseudocapacitive contributions of ca. 47, 57, 71 and 86 % at scan rates of 0.2, 0.5, 2, and 5 mV s^{-1}, respectively. In contrast, the Li-ion system features significantly higher diffusion-limited contributions although a similar increase in pseudocapacitive contributions is observed, with pseudocapacitive percentage contributions of 32, 41, 58, and 74 % at scan rates of 0.2, 0.5, 2, and 5 mV s^{-1}, respectively.

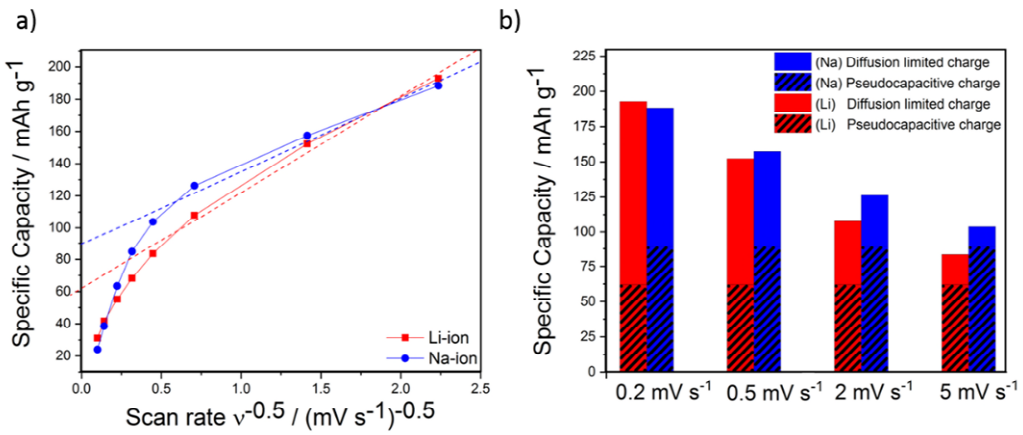

Figure 5. (a) Trasatti plot for electrodes of sodium titanate nanopowder (heat-treated at 150 °C). (b) Pseudocapacitive contributions (striped, blue and red) to total specific charge at scan rates of 0.2, 0.5, 2 mV s^{-1}, and 5 mV s^{-1} for electrodes incorporating the sodium titanate nanopowder (heat-treated at 150 °C), in Na-ion half cells (blue) and Li-ion half cells (red), respectively.

Pseudocapacitive behaviour in titanate electrodes has been previously observed in the literature that were attributed to their large surface area and interlayer spacing (ca. 8 Å), giving rise extrinsic (morphological and size dependent) pseudocapacitive characteristics.[70] When comparing Li- and Na-ion behaviours, the greater preference for insertion processes in the Li-ion cell, might be related to the relatively smaller dimensions of the Li-ions (ionic radius of Li = 0.76 Å vs. Na = 1.02 Å).[13] Under such a context, our results are not surprising.

The highly pseudocapacitive nature coupled with a small diffusion-limited insertion component of the titanate electrode herein is reminiscent of compounds such as Nb_2O_5, where insertion-based 2D transport of Li-ions occurs for at the near-surface nanoparticles without any accompanying phase change, in what is termed "intercalation pseudocapacitance".[66] Materials such as $LiCoO_2$ and V_2O_5 are known to exhibit an almost linear dependence between voltage and stored charge when nano-sized.[71, 72] This is thought to originate from the formation "solid-solution" of surface sites available for ionic insertion across a wide range of energies, once a critical crystallite size was reached. This variance in site energy is due to the inherent structural disorder observed for surface atoms, and changes with the concentration of ions inserted on to the surface, resulting in a linearly sloped voltage profile being observed. The linear relationship between cell potential and stored charge was investigated for electrodes of the sodium titanate active material (heat-treated at 150 °C) through voltage profiles at a relatively low specific current of 50 mA g^{-1} for the first two cycles for both Li- and Na-ion systems (Figure 6).

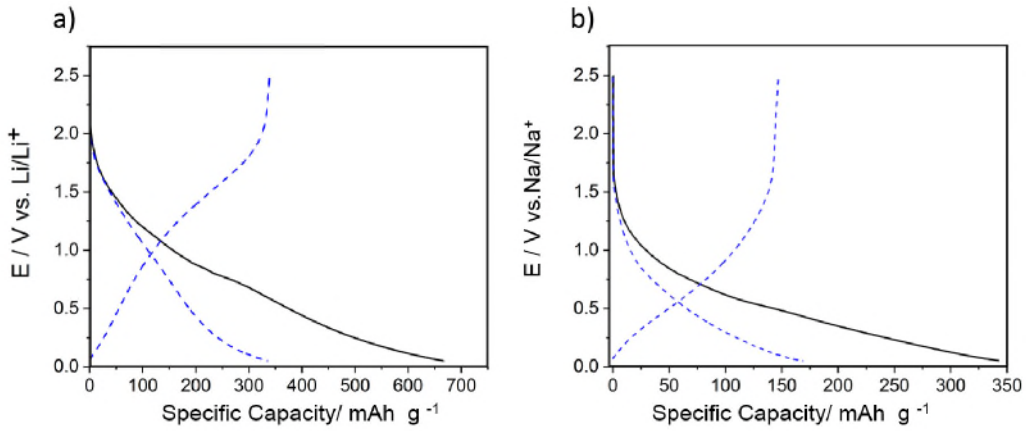

Figure 6. Potential versus specific capacity profile for the half-cells made from electrodes containing sodium titanate (heat-treated at 150 °C) at a specific current of 100 mA g^{-1}(a) in Li-ion half-cells in the range 0.1 to 2.5 V vs. Li/Li^+ and (b) in Na-ion half-cells in the range 0.1 to 2.5 V vs. Na/Na^+. First cycle discharge shown in black, and second cycle charge-discharge shown in dashed blue.

Overall, an almost linear dependence was observed between potential and stored charge for both Li- and Na-ion systems, a characteristic trait usually seen for pseudocapacitive charge storage.[73] This is in direct contrast to traditional bulk materials exhibiting single voltage plateaus or two-phase insertion mechanism previously described in literature where two separate plateaus were observed that corresponded to the shift from $Na_2Ti_3O_7$ to $Na_{3-x}Ti_3O_7$ and then to $Na_4Ti_3O_7$.[55, 74, 75] This difference has been attributed to the large particle size differences, with larger particles adopting more bulk-material behaviour and nano-sized sodium titanate (heat-treated at 150 °C) showing a reduced or no miscibility gap when accommodating Na-ions. This suggested that the half-cell containing the nanopowder electrode herein was behaving as an extrinsic pseudocapacitor in Na-ion systems.[71] Similar behaviour has been seen in the literature for other materials such as nano-TiO_2, and has been ascribed to the very small diffusion distances that are characteristic of nano-sized electrode materials.[76]

The specific capacities at various specific currents were investigated in both Li-ion and Na-ion half-cells (10 cycles per each applied specific current), with the results plotted in Figure 7. The high drop in capacity during the initial cycles for the Na-ion cell was attributed to the irreversible sodiation of the carbon black and the formation of the SEI by Xu et al.[77] The resulting lower reversible capacity was

ascribed to both the formation of the SEI or other reactions involving the decomposition of surrounding $LiPF_6$ or $NaPF_6$ electrolyte, respectively.[52, 77]

Both the Li-ion and Na-ion cells of sodium titanate nanopowder heat-treated at 150 °C displayed high Coulombic efficiencies > 99 % after 20 cycles. For the Li-ion half-cell at specific currents of 50 (~0.3 C, where 1 C refers to the applied specific current needed to charge and discharge the cell to full theoretical capacity in one hour), 100 (~0.6 C), and 200 (~1.1 C) mA g^{-1}, specific capacities of ca. 260, 235, and 205 mAh g^{-1}, respectively, were achieved. At higher specific currents of 750 (~4.2 C), 1000 (~5.6 C) and 2000 (~11.3 C) mA g^{-1}, the corresponding capacities were 160, 150 and 128 mAh g^{-1}, respectively, before recovering back to 243 mAh g^{-1} at a specific current of 50 mA g^{-1}. For the Na-ion half-cell, at the same low specific currents (50, 100, and 200 mA g^{-1}, corresponding to 0.3, 0.6, and 1.1 C, respectively) specific capacities of 152, 135, and 117 mA g^{-1}, respectively, were observed. At higher specific currents (750, 1000 and 2000 mA g^{-1}, corresponding to 4.2, 5.6, and 11.3 C, respectively) the capacities were 100, 95 and 83 mAh g^{-1}, respectively, before recovering back to 131 mAh g^{-1} at a specific current of 50 mA g^{-1}. The observed decrease in performance for all cells at high specific currents has been ascribed to kinetically-limited diffusion processes, although the larger size of the Na-ion versus Li-ions compared to the titanate interlayer spacing (ca. 8 Å)[18], may also have a role at limiting ionic diffusion for Na-ions at high specific currents.[78]

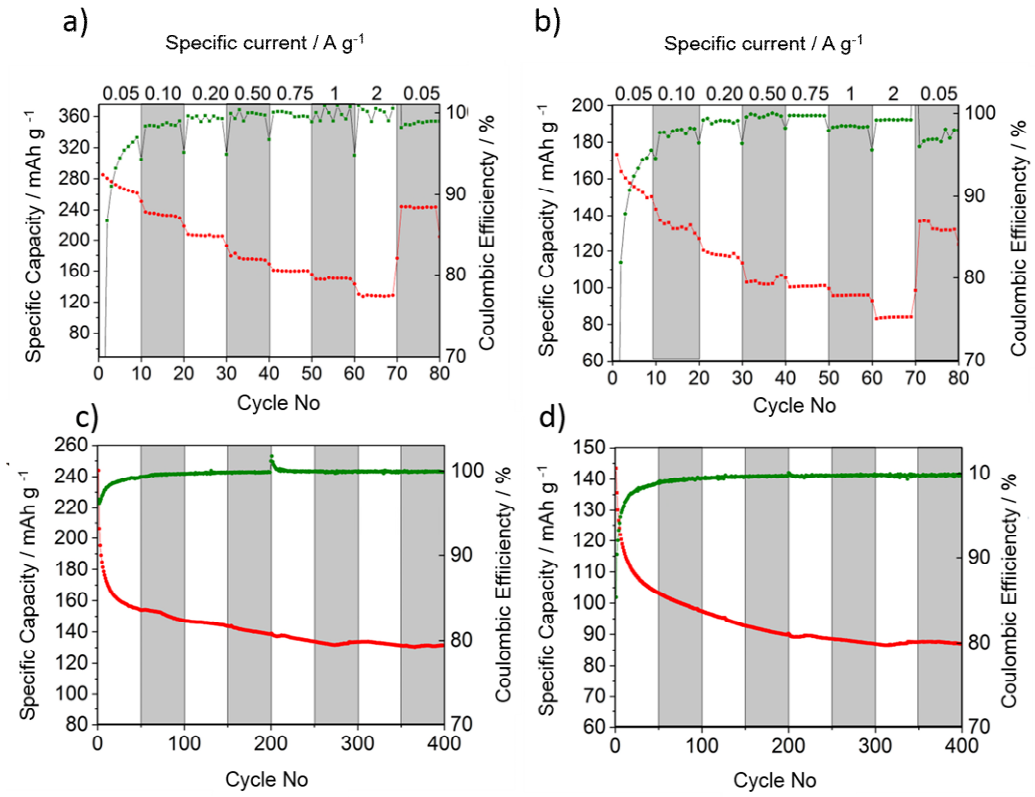

Figure 7. (Top) Rate tests for half-cells containing electrodes made from sodium titanate nanopowder (heat-treated at 150 °C); the cells were cycled at specific currents of 50, 100, 200, 500, 750, 1000, 2000, and 50 mA g^{-1} for 10 cycles each for (a) a Li-ion cell in the potential range 0.1 to 3.0 V vs. Li/Li^+ and (b) a Na-ion cell in the potential range 0.1 to 2.5 V vs. Na/Na^+. (Bottom) Long-term galvanostatic charge-discharge cycling tests (400 cycles) at a specific current of 1000 mA g^{-1} for the (c) Li-ion and (d) Na-ion cells. Specific capacities (red) displayed with Coulombic efficiencies (green).

Following the rate tests, long-term galvanostatic charge-discharge cycling tests at a specific current of 1000 mA g^{-1} for 400 cycles for both the Li- and Na-ion half-cells. Following a slow decay for ca. 300 cycles, capacities stabilized at ca. 131 and 87 mA g^{-1} for 1000 mA g^{-1} for Li-ion and Na-ion cells, respectively, with high Coulombic efficiencies of > 99 %. The results at the end of the 300th cycle represented only a ca. 23 and 25 % decrease in charge storage capacities from those of the 10th cycle, indicating good charge retention capabilities for the Li- and Na-ion half cells, respectively. As, previously mentioned, the significant drop in first cycle-capacity can be attributed to the formation of the SEI layer, along with various other parasitic side reactions at the surface level. Such first cycle losses have been addressed in literature through the use of presodiation, prelithiation, along with

different electrolyte additives such as cyclohexane, nitrate, vinylene carbonate, and fluoroethylene carbonate. These additives are known to facilitate the formation of a more stable SEI layer through either limiting the participation of electrons in side reactions, or by removing unstable intermediates to create more stable SEI components.[79-81]

A plot of reported rate performances for selected reports of hydrothermally made $Na_2Ti_3O_7$ and $Na_2Ti_6O_{13}$, and TiO_2 materials is shown in Figure 8. In literature, sodium titanate synthesized via batch hydrothermal methods have shown varying performance depending on particle morphologies. In Li-ion cells, micron-sized $Na_2Ti_6O_{13}$ tubes synthesized via a batch hydrothermal and calcination by Dominko et al., exhibited reversible capacities of 150 mAh g^{-1} at a specific current of only 5 mA g^{-1}, while batch hydrothermal synthesis of titanate nanotubes by Zhang et al. achieved much higher capacities of 135 mAh g^{-1} at 50 mA g^{-1} in a Li-ion half-cell.[82, 83] Lubke et al. synthesized $Na_{0.9}H_{1.1}Ti_3O_7$ via a continuous hydrothermal process, obtaining high reversible capacities of 150 and 125 mAh g^{-1} for specific currents of 50 and 500 mA g^{-1}, respectively (Li-ion half-cell).[23] The superior performance of the titanate material reported herein, notably outperforms all of them as evidenced by the higher capacities of 260 and 160 mAh g^{-1} at 50 and 750 mA g^{-1}. This advantage may originate from its higher proportion of inter-layer Na-ions (formula herein was suggested as $Na_{1.5}H_{0.5}Ti_3O_7$), facilitating the creation of greater and more stable 2D- channels for Li-ion insertion processes.

For Na-ion, the electrochemical results reported herein are in agreement with similar materials obtained in the comparable batch hydrothermal synthesis literature.[25, 84] $Na_2Ti_3O_7$ made via batch hydrothermal methods at high base concentrations have been used to make half cells with capacities of 72 mAh g^{-1} at a specific current of 40 mA g^{-1}, while $NaTi_3O_6(OH)_2 \cdot H_2O$ that was made via a one-step batch hydrothermal synthesis, exhibited a specific capacity of 100 mAh g^{-1} at 30 mA g^{-1} (when dehydrated post-synthesis before making into an electrode).[19, 28] Mixed-phase $Na_2Ti_3O_7$ and $Na_2Ti_6O_{13}$ titanate heat-treated at 800 °C by Vanek et al. was used in an anode and displayed capacities of 63 mAh g^{-1} at a specific current of 39 mA g^{-1}, while electrodes made using $Na_2Ti_3O_7$ annealed at 850°C, yielded capacities of 72 and 58 mAh g^{-1} at specific currents of 40 and 200 mA g^{-1}, respectively.[85, 86] Similarly at high specific currents, anodes incorporating $Na_2Ti_3O_7$ nanotubes made

by Wang et al. exhibited high capacities of 108 mAh g^{-1} at a high specific current of 354 mA g^{-1} (2 C, or the theoretical rate required to fully charge the cell in half an hour) in Na-ion half-cells. In comparison, Rudola et al. obtained capacities of ca. 80 mAh g^{-1} at a specific current of ca. 600 mA g^{-1}) in Na-ion half-cells. [50, 87]. Therefore, the higher capacities of 152 and 100 mAh g^{-1} at 50 and 750 mA g^{-1} from our anodes incorporating sodium titanate nanopowder, dislay clear advantages.

In the literature, $Na_2Ti_3O_7$ has usually been shown to perform marginally worse than batch hydrothermally-synthesized TiO_2 (B), anatase, and CHFS-synthesized anatase, which can be attributed to the higher number of Li- and Na-ion insertion sites within their unit cells accompanied by a larger gravimetric energy density: for example, TiO_2 (B) possesses a high theoretical capacity of 335 mAh g^{-1}.[49, 67, 88-91] Hydrothermally-made TiO_2 (B) and anatase have delivered capacities of 107 mAh g^{-1} and 177 mAh g^{-1} at specific currents of 100 and 84 mA g^{-1}, respectively, in Na-ion cells [6, 90, 92] In Li-ion cells, hydrothermally synthesized TiO_2 (B) has exhibited capacities of 200 mAh g^{-1} at a specific current of 200 mA g^{-1}, while anatase TiO_2 nanotubes have shown capacities of 182 mAh g^{-1} at a specific current of 180 mA g^{-1}.[89, 91]

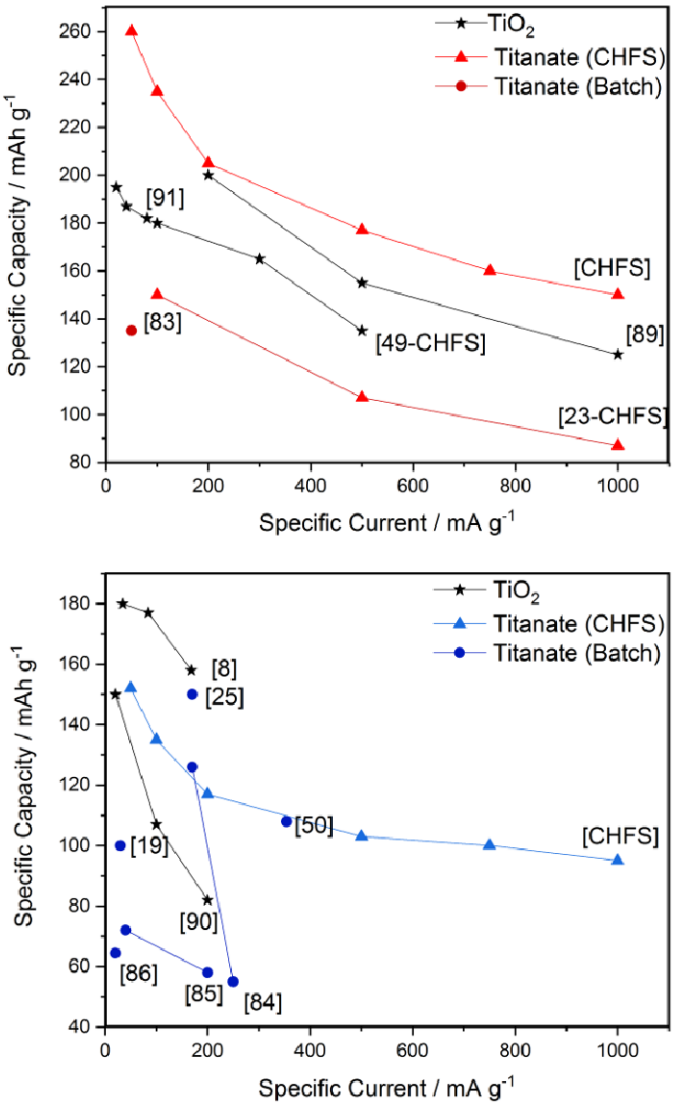

Figure 8. Plot of charge capacities versus specific current of selected anodes made using titanate and titania materials, synthesized via hydrothermal methods. (a) Blue circles and triangles refers to results obtained for titanates in Na-ion half cells, (b) red triangle and circles are for results obtained in Li-ion, and black stars are the results obtained for TiO_2 polymorphs in the corresponding system. Numbers in square brackets are the corresponding reference numbers.

4. Conclusions

Layered phase-pure sodium titanate nanopowder with composition $Na_{1.5}H_{0.5}Ti_3O_7$ was synthesised at relatively low base concentration of only 4 M using a continuous hydrothermal flow synthesis process at a production rate of 62 g per hour. The material was heat treated at 150 °C and used as an active electrode material in both Na-ion and Li-ion half-cells. The crystal structure, small crystallite size, and high surface area of the titanate material, resulted in high overall specific capacities with contributions from both pseudocapacitive surface effects as well as insertion processes. It was possible to obtain a specific capacity of 135 and 235 mAh g^{-1} at a specific current of 100 mA g^{-1} for Na- and Li-ion systems, respectively. Both Na- and Li-ion systems exhibited a combination of diffusion-limited and pseudocapacitive charge storage mechanisms, with increasing contributions from the latter suggested to occur with higher scan rates the long-term high-power performance for over 400 cycles for this active material was also relatively stable, giving capacities of ca. 83 and 131 mAh g^{-1} at a specific current of 1000 mA g^{-1}, with high Coulombic efficiency of 99 %. Given that sodium titanate materials have been shown to exhibit adequate insertion behaviour in aqueous electrolytes, we believe it worth investigating if a difference in pseudocapacitance can be observed by our nanomaterial in aqueous systems.[93] Finally, the feasibility of examining (carbon-coated) titanate production utilizing a scaled-up CHFS pilot plant will be examined in the future.

Acknowledgements

The Engineering and Physical Sciences Research Council are thanked for funding the Centre for Doctoral Training in Molecular Modelling & Materials Science (UCL, UK; EPSRC reference EP/L015862/1) and IMRE & A*STAR (Agency for Science, Technology and Research) are thanked for supporting a studentship for YX. The authors also thank EPSRC for funding The JUICED Hub (Joint University Industry Consortium for Energy (Materials) and Devices Hub, EP/R023662/1). Dr Liam McCafferty (funded under EPSRC EP/R023662/1) is thanked for his expertise and support in this project.

Notes and references

---

[1] J. Li, X. Wang, Energy Pol., 41 (2012) 519-528.
[2] P. Taylor, in, Institute of Sustainability, Newcastle University, 2015. (http://www.ncl.ac.uk/media/wwwnclacuk/instituteforsustainability/files/Energy%20Policy%20Briefing%20Note.pdf, *accessed 04.07.2018*)
[3] M.R. Palacin, Chem. Soc. Rev., 38 (2009) 2565-2575.
[4] S.W. Kim, D.H. Seo, X. Ma, G. Ceder, K. Kang, Adv. Energy Mater., 2 (2012) 710-721.
[5] R.C. Masse, E. Uchaker, G. Cao, Sci. China. Mater., 58 (2015) 715-766.
[6] L. Wu, D. Buchholz, D. Bresser, L. Chagas, S. Passerini, J. Power Sources (2014) 379-385.
[7] D.J. Cloyd, in: U.S.P. Office (Ed.), United States Patent 1501756, 1924.
[8] S.F. Skala, in: U.S.P. Office (Ed.), United States Patent 4276145, 1981.
[9] H.N. Gilbert, J. Electrochem. Soc, 99 (1952) 305-306.
[10] Q. Ni, Y. Bai, F. Wu, C. Wu, Adv. Sci., 4 (2017) 1600275.
[11] Y. Cao, L. Xiao, M.L. Sushko, W. Wang, B. Schwenzer, J. Xiao, Z. Nie, L.V. Saraf, Z. Yang, J. Liu, Nano letters, 12 (2012) 3783-3787.
[12] J. Libich, M. Kundu, O. Cech, M. Sedlarikova, J. Vondrak, P. Cudek, J. Maca, ECS Trans., 74 (2016) 313-319.
[13] D.R. Lide, CRC Handbook of Chemistry and Physics, 84th edtion ed., CRC, Boca Raton, 2004.
[14] D. Kundu, E. Talaie, V. Duffort, L.F. Nazar, Angew. Chem. Int. Ed., 54 (2015) 3431-3448.
[15] T. Adschiri, K. Kanazawa, K. Arai, J. Am. Ceram. Soc, 75 (1992) 1019-1022.
[16] P. Boldrin, A.K. Hebb, A.A. Chaudhry, L. Otley, B. Theibaut, P. Bishop, J.A. Darr, Ind. Eng. Chem. Res., 46 (2007) 4830-4838.
[17] C. Bommier, X. Ji, Isr. J. Chem., 55 (2015) 486-507.
[18] L. Zennaro, M. Magro, F. Vianello, A. Rigo, G. Mariotto, M. Giarola, E. Froner, M. Scarpa, Chem. Phys. Chem., 14 (2013) 2786- 2792.
[19] M. Shirpour, J. Cabana, M. Doeff, Energy Environ. Sci., 6 (2013) 2538-2547.
[20] S. Chauque, C.B. Robledo, E.P.M. Leiva, F.Y. Oliva, O.R. Cámara, ECS Trans., 63 (2014) 113-128.
[21] P. Senguttuvan, G. Rousse, V. Seznec, J.M. Tarascon, M.R. Palacin, Chem. Mater., 23 (2011) 4109-4111.
[22] R. Aziz, I. Misnon, K.F. Chong, M. Yusoff, R. Jose, Electrochim. Acta, 113 (2013) 141-148.
[23] M. Lubke, P. Marchand, D. Brett, P. Shearing, R.I. Gruar, Z. Liu, J.A. Darr, J. Power Sources, 305 (2016) 115-121.
[24] J. Wang, J. Polleux, J. Lim, B. Dunn, J. Phys. Chem. C. , 111 (2007) 14925- 14931.
[25] L. Zhao, L. Qi, H. Wang, J. Power Sources, 242 (2013) 597-603.
[26] R. Gruar, C.J. Tighe, L.M. Reilly, G. Sankar, J.A. Darr, Solid State Sci., (2010) 1683-1686.
[27] J.A. Darr, J. Zhang, N.M. Makwana, X. Weng, Chem. Rev., 117 (2017) 11125-11238.
[28] O. Cech, P. Vanysek, L. Chladil, K. Castkova, ECS Trans., 74 (2016) 331-337.
[29] L. Shi, A.J.T. Naik, J.B.M. Goodall, C.J. Tighe, R. Gruar, R. Binions, I. Parkin, J.A. Darr, Langmuir, 29 (2013) 10603-10609.
[30] S. Elouali, L.G. Bloor, R. Binions, R. Parkin, C.J. Carmalt, J.A. Darr, Langmuir, 28 (2012) 1879-1885.
[31] C. Xu, J. Lee, A.S. Teja, J. of Supercritical Fluids, 44 (2008) 92-97.

[32] Z. Zhang, J.B.M. Goodall, D.J. Morgan, S. Brown, R.J.H. Clark, J.C. Knowles, N.J. Mordan, J.R.G. Evans, A.F. Carley, M. Bowker, J.A. Darr, J. Eur. Ceram. Soc., 29 (2009) 2343-2353.
[33] P.W. Dunne, A.S. Munn, C.L. Starkey, T.A. Huddle, E.H. Lester, Phil. Trans. R. Soc. A 3, 373 (2015) 20150015.
[34] Z. Zhang, J.B.M. Goodall, S. Brown, L. Karlsson, R.J.H. Clark, J.L. Hutchison, I.U. Rehman, J.A. Darr, Dalton Trans., 39 (2010) 711-714.
[35] X. Weng, P. Boldrin, I. Abrahams, S.J. Skinner, J.A. Darr, Chem. Mater., 19 (2007) 4382-4384.
[36] J.A. Darr, M. Poliakoff, Chem. Rev., 99 (1999) 495-541.
[37] R.I. Gruar, C.J. Tighe, J.A. Darr, Ind. Eng. Chem. Res., 52 (2013) 5270-5281.
[38] M. Chen, C.Y. Ma, T. Mahmud, J.A. Darr, X.Z. Wang, J. Supercrit. Fluids, 59 (2011) 131-139.
[39] C.J. Tighe, R.Q. Cabrera, R.I. Gruar, J.A. Darr, Ind. Eng. Chem. Res., 16 (2013) 5522-5528.
[40] X.L. Weng, B. Perston, X.Z. Wang, I. Abrahams, T. Lin, S.F. Yang, J.R.G. Evans, D.J. Morgan, A.F. Carley, M. Bowker, J.C. Knowles, I. Rehman, J.A. Darr, Appl. Catal., B., 90 (2009) 405-415.
[41] X. Weng, P. Boldrin, Z. Zhang, J.A. Darr, Clean Technol. 2008: Bio Energy, Renew., Green Build., Smart Grid, Stor. Water, (2008) 261-264.
[42] X. Weng, J. Zhang, Z. Wu, Y. Liu, H. Wang, J.A. Darr, Appl. Catal., B., 103 (2011) 453-461.
[43] R.I. Gruar., C.J. Tighe, J. Muir, J.T. Kittler, M. Wodjak, A.J. Kenyon, J.A. Darr, RSC Adv., 2 (2012) 10037-10047.
[44] M.J. Powell, P. Marchand, C.J. Denis, J.C. Bear, J.A. Darr, I.P. Parkin, Nanoscale, 7 (2015) 18686-18693.
[45] R.I. Gruar, C.J. Tighe, P. Southern, Q.A. Pankhurst, J.A. Darr, Ind. Eng. Chem. Res., 54 (2015) 7436-7451.
[46] P. Marchand, N.M. Makwana, C.J. Tighe, R.I. Gruar, I.P. Parkin, C.J. Carmalt, J.A. Darr, ACS. Comb. Sci., 18 (2016) 130-137.
[47] R.I. Gruar, C.J. Tighe, J.A. Darr, in, US, 2015.
[48] C.J. Denis, C.J. Tighe, R.I. Gruar, N.M. Makwana, J.A. Darr, Cryst. Growth Des., 15 (2015) 4256-4265.
[49] M. Lübke, I. Johnson, N.M. Makwana, D. Brett, P. Shearing, Z. Liu, J.A. Darr, J. Mater. Chem. A., 3 (2015) 22908-22914.
[50] W. Wang, C. Yu, Y. Liu, J. Hou, H. Zhu, S. Jiao, Nanoscale, (2012) 594-599.
[51] A.L. Patterson, Phys. Rev., 56 (1939) 978.
[52] Z. Yan, L. Liu, H. Shu, X. Yang, H. Wang, J. Tan, Q. Zhou, Z. Huang, X. Wang, J. Power Sources, 274 (2015) 8-14.
[53] Z. Zhang, S. Brown, J.B.M. Goodall, X. Weng, K. Thompson, K. Gong, S. Kellici, R.J.H. Clark, J.R.G. Evans, J.A. Darr, J. Alloys Compd. , 476 (2009) 451-456.
[54] Q. Chen, W. Zhou, G. Du, L.M. Peng, Adv. Mater. , 14 (2002) 1208-1211.
[55] Z. Zhou, H. Xiao, F. Zhang, X. Zhang, Y. Tang, Electrochim. Acta, 211 (2016) 430-436.
[56] P. Umek, R.C. Korošec, B. Jančar, R. Dominko, D. Arčon, J. Nanosci. Nanotechnol., 7 (2007) 3502-3508.
[57] Y.V. Kolenko, K.A. Kovnir, A.I. Gavrilov, A.V. Garshev, J. Frantti, O.I. Lebedev, B.R. Churagulov, G. Van Tendeloo, M. Yoshimura, J. Phys. Chem. B., 110 (2006) 4030-4038.
[58] S. Papp, L. Kõrösi, V. Meynen, P. Cool, E.F. Vansant, I. Dékány, J. Solid State Chem., 178 (2005) 1614-1619.
[59] P.K. Allan, M. Tsiamtsouri, C. Grey, A. Pell, J. Stratford, G. Kim, R. Kerber, P. Magusin, D. Jefferson, Chem. Mater., 5 (2018) 1505-1516.
[60] U. Holzwarth, N. Gibson, Nature Nanotech., 6 (2011) 534.
[61] J. Zhu, J. Yang, Z.-F. Bian, J. Ren, Y.-M. Liu, Y. Cao, H.-X. Li, H.-Y. He, K.-N. Fan, ACS Appl. Catal. B., 76 (2007) 82-91.
[62] J.S. Ko, V.V. Doan-Nguyen, H.-S. Kim, G.A. Muller, A.C. Serino, P.S. Weiss, B.S. Dunn, ACS Appl. Mater. Interfaces, 9 (2017) 1416-1425.
[63] R.A. Zarate, S. Fuentes, J.P. Wiff, V.M. Fuenzalida, A.L. Cabrera, J. Phys. Chem. Solids, 68 (2007) 628-637.

[64] D. Yang, Z. Zheng, H. Liu, H. Zhu, X. Ke, Y. Xu, D. Wu, Y. Sun, J. Phys. Chem. C, 112 (2008) 16275-16280.
[65] W. Chen, X. Guo, S. Zhang, Z. Jin, J. Nanopart. Res, 9 (2006) 1173-1180.
[66] J. Come, V. Augustyn, J.W. Kim, P. Rozier, P. Taberna, P. Gogotsi, J. Long, B. Dunn, P. Simon, J. Electrochem. Soc., 161 (2014) A718-A725.
[67] A.G. Dylla, G. Henkelman, K. Stevenson, Acc. Chem. Res. , 46 (2013) 1104-1112.
[68] S. Ardizzone, G. Fregonara, S. Trasatti, Electrochim. Acta, 35 (1990) 263-267.
[69] C. Liu, E. Gillette, X. Chen, A.J. Pearse, A.C. Kozen, M.A. Schroeder, K.E. Gregorczyk, S.B. Lee, G.W. Rubloff, Nature Nanotech., 9 (2014) 1031-1039.
[70] J. Li, Z. Tang, Z. Zhang, Chem. Mater., 17 (2005) 5848-5855.
[71] M. Okubo, E. Hosono, J. Kim, M. Enomoto, N. Kojima, T. Kudo, H. Zhou, I. Honma, J. Am. Chem. Soc., 129 (2007) 7444-7452.
[72] M. Sathiya, A.S. Prakash, K. Ramesha, J.M. Tarascon, A.K. Shukla, J. Am. Chem. Soc., 133 (2011) 16291-16299.
[73] V. Augustyn, P. Simon, B. Dunn, Energy Environ. Sci., 7 (2014) 1597-1614.
[74] A. Rudola, N. Sharma, P. Balaya, Electrochem. Commun., 61 (2015) 10-13.
[75] M. Cabello, G.F. Ortiz, M.C. López, P. Lavela, R. Alcántara, J.L. Tirado, Electrochemistry Communications, 56 (2015) 61-64.
[76] Y. Xu, E.M. Lotfabad, H. Wang, B. Farbod, Z. Xu, A. Kohandehghan, D. Mitlin, Chem. Commun., 49 (2013) 8973-8975.
[77] J. Xu, C. Ma, M.B. Lasubramanian, Y.S. Meng, Chem. Commun, 50 (2014) 12564-12567.
[78] Y. Tang, Y. Zhang, W. Li, B. Ma, X. Chen, Chem. Soc. Rev., 44 (2015) 5926-5940.
[79] J. Deng, W.B. Luo, S.L. Chou, H.K. Liu, S.X. Dou, Advanced Energy Materials, 8 (2018) 1701428.
[80] S.S. Zhang, Journal of Power Sources, 162 (2006) 1379-1394.
[81] Y. Sun, H.-W. Lee, Z.W. Seh, N. Liu, J. Sun, Y. Li, Y. Cui, Nature Energy, 1 (2016) 15008.
[82] R. Dominko, E. Baudrin, P. Umek, D. Arčon, M. Gaberšček, J. Jamnik, Electrochem. Commun., 8 (2006) 673-677.
[83] H. Zhang, X.P. Gao, G.R. Li, T.Y. Yan, H.Y. Zhu, Electrochim. Acta., 53 (2008) 7061-7068.
[84] L. Zhao, L. Qi, H. Wang, ACS Appl. Mater. Interfaces, 4 (2012) 2762–2768.
[85] P. Posch, in: Institute for Chemistry and Technology of Materials, Graz University of Chemistry, 2016.
[86] M. Vanek, in: Department of Electrical and Electronic Technoloy, Brno University of Technology, 2016.
[87] A. Rudola, K. Saravanan, S. Devaraj, H. Gong, P. Balaya, J. Mater. Chem. A, 1 (2013) 2653-2662.
[88] X. Yang, C. Wang, Y. Yang, Y. Zhang, X. Jia, J. Chen, X. Ji, J. Mater. Chem. A., 3 (2015) 8800-8807.
[89] A.R. Armstrong, G. Armstrong, J. Canales, R. García, P.G. Bruce, Adv. Mater., 17 (2005) 862-865.
[90] J. Lee, J.K. Lee, K.Y. Chung, H. Jung, H. Kim, J. Mun, W. Choi, Electrochim. Acta, 200 (2016) 21-28.
[91] Y. Zhou, L. Cao, F. Zhang, B. He, H. Li, J. Electrochem. Soc., 150 (2003) A1246-A1249.
[92] D. Wu, X. Li, B. Xu, N. Twu, L. Liu, G. Ceder, Energy Environ. Sci., 8 (2015) 195-202.
[93] M. Cabello, G.F. Ortiz, M.C. López, R. Alcántara, J.R. González, J.L. Tirado, R. Stoyanova, E. Zhecheva, J. Alloys Compd., 646 (2015) 816-826.